National Aeronautics and Space Administration

Orbital Debris Quarterly News

Volume 27, Issue 1
March 2023

Inside...

A publication of the NASA Orbital Debris Program Office (ODPO)

Two More On-orbit Fragmentations in 2022

The 18th Space Defense Squadron (18 SDS) of the U.S. Space Force detected two on-orbit fragmentations during the last quarter of 2022: a major upper stage breakup and the breakup of mission-related debris.

The first was a major breakup of a Long March 6A (CZ-6A) upper stage (International Designator 2022151B, Catalog Number 54236) associated with the launch of China's Yunhai-3 weather satellite. The dry mass of the upper stage is approximately 5800 kg. Shortly after the deployment of Yunhai-3, the upper stage experienced a breakup at around 05:24 to 05:29 GMT on 12 November 2022. At the time of the breakup, the apogee altitude, perigee altitude, and inclination of the upper stage were approximately 847 km, 813 km, and 98.8 degrees, respectively.

By the end of January 2023, the 18 SDS had identified and cataloged 533 CZ-6A fragments based on data collected by the Space Surveillance Network (SSN). The Gabbard diagram indicates that most of the fragments are concentrated between 600 km and 1000 km altitudes, with a spread from approximately 300 km to 1600 km altitudes. Data from past ground-based observations and laboratory impact experiments has shown that breakup fragments follow a power-law size distribution – indicating there is more small debris than large. Fragments large enough to be detected and cataloged by the SSN only represent the tip of the iceberg. Hundreds of thousands of fragments as small as one millimeter in size were likely generated from this breakup. Because of the high altitude of the event, the 2022-151B CZ-6A fragments will have nontrivial, long-term, negative effects

continued on page 2

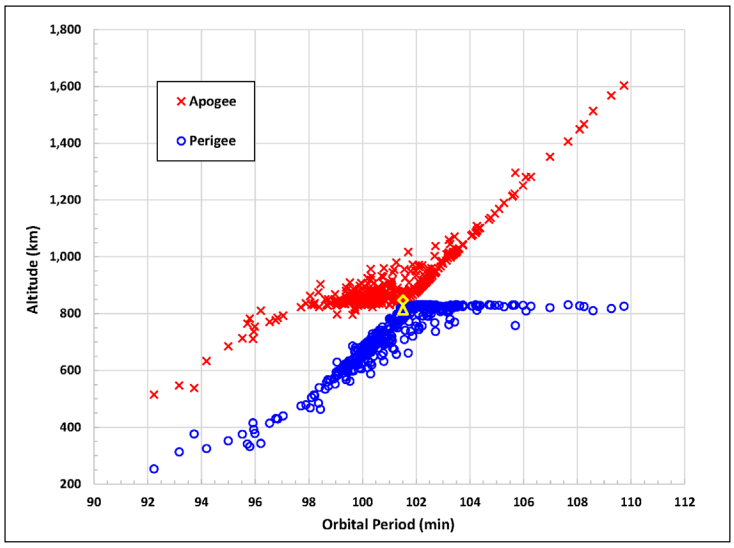

A Gabbard diagram of the 2022-151B CZ-6A fragments, based on catalog elements dated 31 December 2022. The apogee (yellow diamond) and perigee (yellow triangle) altitudes of the parent upper stage are also shown.

More 2022 Fragmentations

continued from page 1

to the environment and to missions operating below about an 1100 km altitude.

The table below ranks the top-10 worst historical breakups by the number of cataloged fragments generated from each event, based on the catalog data as of 31 January 2023. The total of 533 fragments places the breakup of the 2022-151B CZ-6A upper stage among the worst in history. This severity underlines the importance of minimizing the probability of accidental explosions associated with upper stages and spacecraft to limit the generation of new fragmentation debris.

The Top-10 Worst Historical Breakup Events Based on Catalog Data as of 31 January 2023

Rank	International Designator	Common Name	Year of Breakup	Apogee Altitude (km)	Perigee Altitude (km)	Debris Cataloged	Debris in Orbit	Assessed Cause of Breakup
1	1999-025A	Fengyun-1C	2007	865	845	3532	2793	Anti-satellite (ASAT) test
2	1982-092A	Cosmos 1408	2021	490	465	1785	364	ASAT test
3	1993-036A	Cosmos 2251	2009	800	775	1715	1021	Accidental collision (with Iridium 33)
4	1994-029B	STEP II upper stage	1996	820	585	754	76	Accidental explosion
5	1997-051C	Iridium 33	2009	780	775	657	300	Accidental collision (with Cosmos 2251)
6	2022-151B	CZ-6A upper stage	2022	847	813	533	529	Accidental explosion
7	2006-026A	Cosmos 2421	2008	420	400	509	0	Unknown
8	1986-019C	SPOT 1 upper stage	1986	835	805	498	30	Accidental explosion
9	1981-053A	Cosmos 1275	1981	1015	960	479	418	Accidental explosion
10	1965-082DM	Titan 3C-4 transtage	1965	790	710	473	32	Accidental explosion

The final on-orbit fragmentation of the year was the breakup of mission-related debris (International Designator 2012-025F, Catalog Number 38345) at 23:36 ± 0:15 GMT on 17 November 2022. This mission-related debris was a cylindrical payload lower fairing panel from a Japanese H-2A upper stage for the deployment of Japan's Global Change Observation Mission (GCOM) W1 Earth observation satellite in 2012. At the time of the breakup, the component's apogee and perigee altitudes were approximately 633 km and 609 km, respectively, with an inclination of 98.2 degrees. The mass of the component is estimated to be more than 100 kg. The 18 SDS had identified and cataloged 30 fragments associated with the breakup at the end of December 2022. Similar breakups associated with other H-2A payload encapsulation system components have been observed before, including one in July 2020 (ODQN, vol. 24, issue 4, November 2020, pp. 1-2) and another in July 2022 (ODQN, vol. 26, issue 3, September 2022, pp. 2). ♦

International Space Station Maneuvers to Avoid Debris for the Third Time in 2022

The International Space Station (ISS) maneuvered to avoid a high-probability collision with a cataloged object for the third time in 2022. The avoided object (International Designator 2011-037PP, Catalog Number 52960) was a piece of fragmentation debris generated from the 2020 breakup of a Russian Fregat upper stage tank (ODQN, vol. 24, issue 3, August 2020, pp. 2-3). This collision avoidance maneuver took place at 13:42 GMT on 21 December 2022, and it raised the apogee and perigee altitudes of the ISS by 2.9 and 0.7 km, respectively. The number of ISS collision avoidance maneuvers against large, tracked objects since 1999 has now reached a total of 33. ♦

NASA Releases History of On-orbit Satellite Fragmentations Update

The NASA Orbital Debris Program Office (ODPO) has released the 16th edition of the History of On-orbit Satellite Fragmentations (HOOSF). This edition succeeds the 15th edition (information cut-off date of 04 July 2018) by updating fragmentation information though 01 May 2022, extending the analysis and description of the orbital debris environment via a decadal survey, and incorporating minor edits and corrections. The 16th edition describes events in three fragmentation categories: breakup events, anomalous events, and aerodynamic events. Breakup events typically feature high-energy separation of fragments from a parent body. Anomalous

continued on page 3

HOOSF Update

continued from page 2

events may feature lower-energy separations (so-called "shedding" events), or their fragment production mechanism is not understood or well characterized by root cause. Aerodynamic breakup events typically occur at or near reentry. These events are categorized separately due to the production mechanism and because they contribute nothing to the orbital environment past the very near term. The figure illustrates the 16th edition's time history of breakup events, generally the most significant event type, from 1960 through 01 May 2022.

Since the 15th edition, there have been 26 identified on-orbit breakups and 9 anomalous events for a historical total of 268 fragmentations and 87 anomalous events. This activity, in addition to launch activity, has resulted in an approximately 21% increase in the number of cataloged space objects since 04 July 2018, including on-orbit and decayed objects, or a 34% increase in on-orbit objects. To better understand the relative implications of recent fragmentations and the launching of large satellite constellations in low Earth orbit (LEO), the 16th edition examined the on-orbit environment in 2001, 2011, 2021, and 2022. In addition, the recent HOOSF release provides insight into the source and sink of breakup debris over the history of the Space Age and compare the continuous removal of debris from the environment and solar activity. Finally, the text explores the occurrence of breakup events by mission phase. These analyses allow the readership to better understand the production and consequences of the orbital debris environment.

The 16th edition of the HOOSF (NASA/TP-20220019160) is available to the public at the NASA ODPO website and the NASA Technical Reports Server. ♦

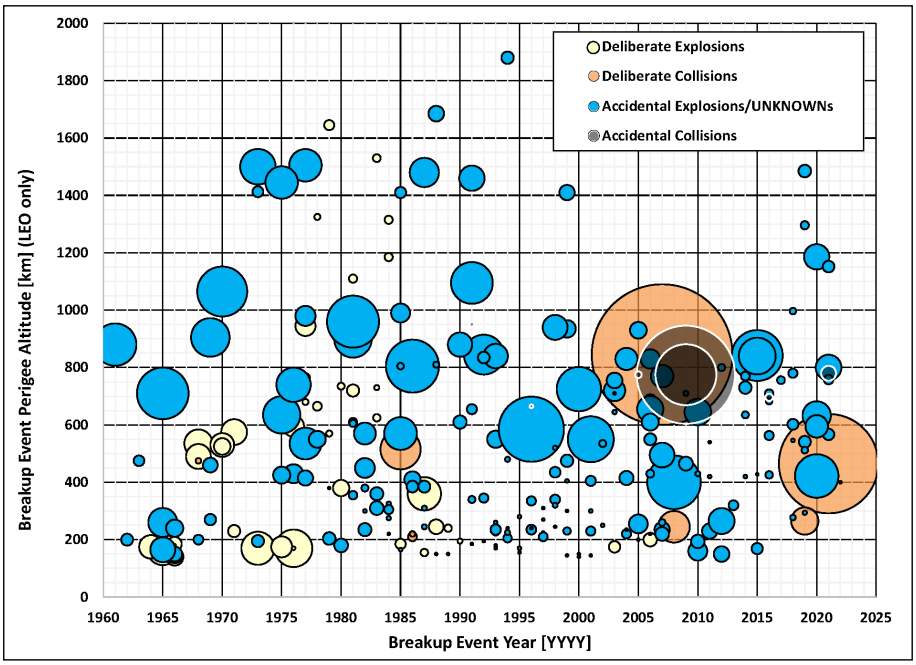

Interpretation of breakup events reported in the 16th HOOSF. Bubbles are centered at the event date and perigee altitude of the parent body, with an area representing the number of catalogued pieces on 01 May 2022. Lower altitude events may have produced many more pieces initially than were ultimately cataloged, and higher altitude events may be similarly undercounted.

Robert C. 'Bob' Reynolds Passes Away

Robert C. Reynolds, the inaugural editor of the NASA Orbital Debris Quarterly News, passed away on 18 June 2022. He received his doctor of philosophy in astronomy from The Ohio State University in 1979, *Evolution of Supermassive Object Accreting Mass,* and was a pioneer in the field of orbital debris. Dr. Reynolds was an early entrant in this field of study, supporting the NASA Orbital Debris Program Office at NASA's Johnson Space Center throughout the 1980s and 1990s. During this time, he made fundamental and significant contributions to measuring, modeling, and mitigating the effects of orbital debris. He worked extensively with radars for general characterization of the environment as well as on specific campaigns, such as observing large rocket bodies upon reentry. In the realm of modeling, he performed significant work characterizing breakup fragmentation events and associated phenomena.

Dr. Reynolds was involved in the development of the Space Station Freedom design environment as well as the evolutionary model EVOLVE, predecessor of the modern LEO to GEO Environment Debris (LEGEND) model. He further explored and developed safety standards and guidelines regarding orbital debris, including sponsoring efforts to characterize the economics of mitigation standard practices. He contributed to domestic and international debris-related efforts, including the early Inter-Agency Space Debris Coordination Committee (IADC). Dr. Reynolds authored or co-authored many technical publications on orbital debris including the book Theory of Satellite Fragmentation in Orbit. In addition to his technical competencies, Dr. Reynolds is remembered for his friendly, welcoming demeanor, his mentorship to the staff, and his collaborative leadership. ♦

PROJECT REVIEW

Updates of the Eugene Stansbery-Meter Class Autonomous Telescope for Geosynchronous Orbit Survey Operations

C. CRUZ, B. BUCKALEW, J. ARNOLD, H. COWARDIN, AND A. MANIS

The Eugene Stansbery-Meter Class Autonomous Telescope (ES-MCAT) has concluded its first survey of the geosynchronous Earth orbit (GEO) region. The goal of the initial survey was to safely collect and autonomously process GEO data with calculated uncertainties. This data will be used for improved characterization of the GEO environment for orbital debris models developed by the NASA Orbital Debris Program Office (ODPO), specifically to update GEO populations in the NASA Orbital Engineering Model (ORDEM).

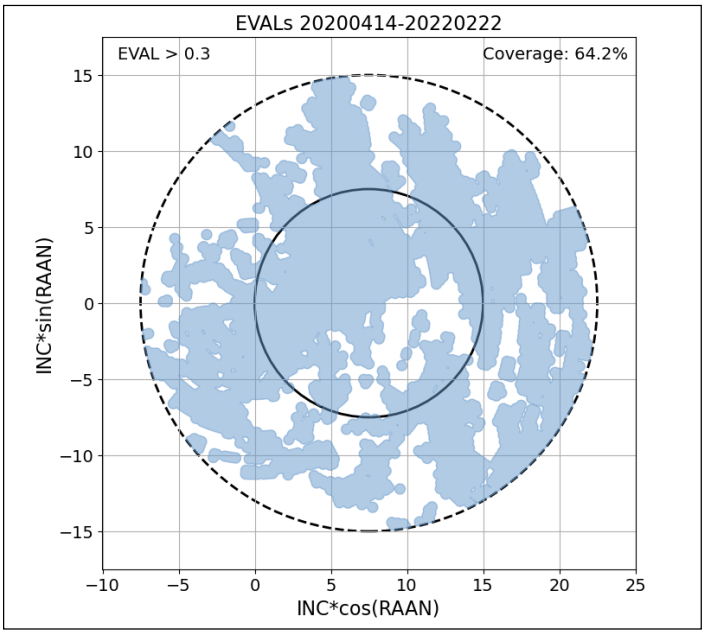

Figure 1. The ROI in Cartesian coordinates (INC·cos(RAAN), INC·sin(RAAN)) shown by the dashed outer circle, and observational expectation values (EVALs) with values greater than 0.3 shown as blue shaded region.

A complete GEO survey with the ES-MCAT is defined as sampling every detectable GEO object's orbit within the region of interest (ROI) that has a certain probability of being sampled, or expectation value (EVAL), during the observation campaign. Based on data utilized from previous sensors, an EVAL of 0.3 was selected as the goal to provide statistically complete coverage over the ROI. This ROI is defined using inclination (INC) and right ascension of the ascending node (RAAN) (ODQN vol. 24, issue 2, April 2020, pp. 4) and traces a circular area in Cartesian coordinates (INC·cos(RAAN), INC·sin(RAAN)), centered at (7.5°, 0°) with a radius of 15°, as shown by the dashed outer circle in Figure 1. The data for the first GEO survey was taken from 14 April 2020 to 22 February 2022 and will be used in ORDEM 4.0 development.

An ODPO-developed prediction and probability coverage software program known as "Tie Dye" calculated the EVALs for given INC and RAAN pairs by using field centers that contain the object's calibrated right ascension (RA), declination (Dec), and the date/time of each observational image as inputs (ODQN, vol. 25, issue 1, February 2021, pp. 2). During the GEO survey, a survey strategy was utilized in an attempt to minimize sampling of historically over-sampled regimes in the ROI (*e.g.*, the region of station-kept GEO spacecraft at (0°, 0°)) and focus on under-sampled regions that are more likely to contain orbital debris. The Tie Dye program determined where to autonomously point the telescope in RA and Dec space at different hours over the duration of the survey to provide adequate coverage of the ROI while accounting for predicted downtime due to insufficient observing conditions. The survey strategy was created, in part, with the Tie Dye program to follow the general shape of the GEO belt and ensure uniform coverage through the INC/RAAN region of interest (ODQN vol. 25, issue 1, February 2021, pp. 3).

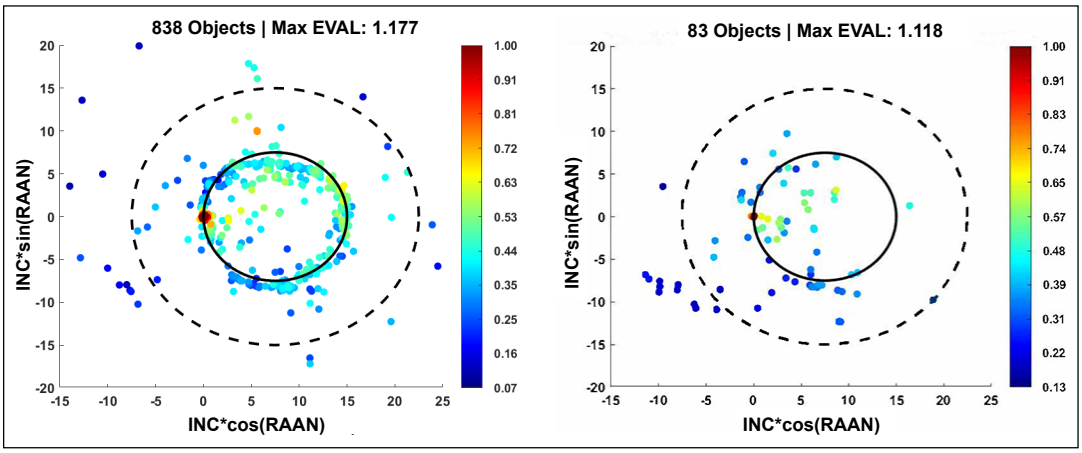

Figure 2. (a) The ROI with each detected CT object plotted as dots, with their color representing the EVAL of the object. (b) The same region of interest with each detected UCT object plotted as multicolored dots.

To estimate the survey's completeness in the ROI, non-photometric nights were simulated in the Tie Dye program. To accommodate for unexpected downtime during the survey (*e.g.*, weather, unscheduled maintenance, or repairs), the ODPO optical team supplemented the survey's autonomous survey pointings with manual survey pointings. With the combination of autonomous pointings and manual additions, 64.2% of the ROI was covered with an EVAL > 0.3 in the first GEO survey with ES-MCAT, as shown in Figure 1.

continued on page 5

ES-MCAT Updates

continued from page 4

The ES-MCAT's daily software routine includes processing and analyses of all previously collected data after each night of observations. The process included applying the photometric and astrometric calibration as well as filtering detections in sequential images to identify GEO objects. Their orbital properties were then propagated to calculate INCs, RAANs, and rates. A match program was utilized to compare detected objects with the satellite catalog available on Space-Track.org. Those that were matched to the catalog are considered correlated targets (CTs) and those not matched are considered uncorrelated targets (UCTs). During the GEO survey, 838 CTs and 83 UCTs were observed. These objects' positions in the Cartesian ROI are shown in Figure 2.

Due to the international travel restrictions caused by the COVID-19 pandemic in 2020 and its remote location, maintenance of the ES-MCAT, including cleaning the primary mirror, was temporarily halted. This temporary lapse in maintenance combined with the harsh sea-level environment of Ascension Island led to galvanic corrosion of the primary reflective surface of the mirror. In preparation for recoating, the primary mirror was removed from the telescope, protected with red First Contact polymer, and secured in a wooden crate for shipping, as shown in Figure 3a. In May 2022, the primary mirror was transported to the ZeCoat Corporation, the vendor responsible for recoating the telescope in 2018 (ODQN vol. 23, issues 1 & 2, May 2019, pp. 3).

As with the previous recoating, ZeCoat Corporation worked closely with the ODPO to develop an improved coating based on the experience gained from operating the facility over the course of the two-year-long GEO survey. The proprietary coating was developed to achieve a minimum 90% reflectivity and enhanced durability to withstand Ascension Island's harsh environment. The final coating was completed on 01 December 2022, shown in Figure 3b, with the reflectance shown in Figure 4.

Figure 3. (a) ES-MCAT's primary mirror with the old reflective coating placed in the shipping crate, ready for transport. A layer of First Contact polymer was applied to the mirror for protection. (b) The primary mirror with a new reflective coating being lowered into the primary mirror cell for installation in the telescope.

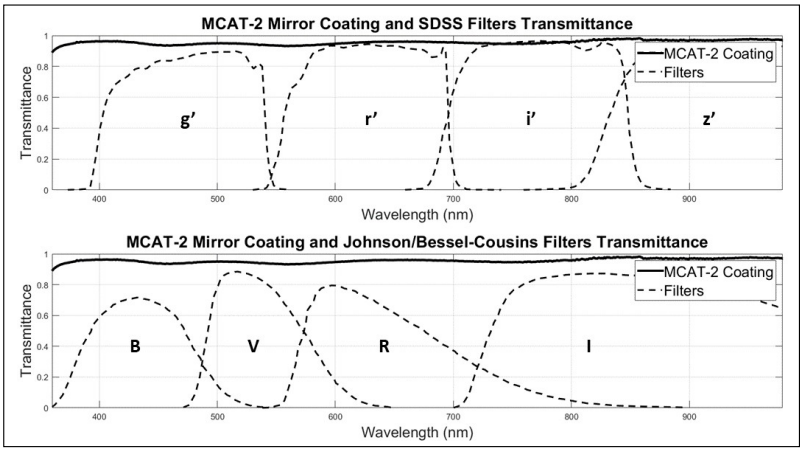

Figure 4. Chart showing ES-MCAT's primary mirror reflectivity with the new (MCAT-2) coating, along with the installed filter transmittance curves.

During the January 2023 trip to Ascension Island, the mirror was re-installed, and an integrated system check-out was performed to ensure the observatory and instruments were ready for data collection in preparation for the next GEO survey to be used with ORDEM. The second GEO survey commenced in January 2023. Filling in the region of interest with an EVAL ≥ 0.3 will continue to be the goal of the GEO surveys while also expanding capabilities that may include calculating orbits with non-zero eccentricities. Future surveys will use insight from the first survey to remove as much downtime as possible while allowing for optimal pointings that better account for the solar phase angle, moon phase, and galactic plane positions, which affect detection capabilities by changing the background noise of the images.

With regular travel to Ascension Island and maintenance of the facility resuming, including regular cleaning of all optical components, the detection capabilities of the ES-MCAT are expected to remain at nominal levels throughout the remainder of the next GEO survey. This will be reflected in the limiting magnitude and minimum detectable size of the system, to be assessed when more data becomes available. In addition to the recent completion of the initial GEO survey and the reinstallation of the re-coated primary mirror, preliminary steps are underway for ES-MCAT to become a contributing sensor to the Space Surveillance Network (SSN).

The ES-MCAT was conceived and funded by both NASA and the Air Force Research Laboratory with a goal of reaching Full Operational Capability (FOC) by proving its ability to safely gather and autonomously process GEO survey data with characterized uncertainties and then transmit the results to Johnson Space Center. With the FOC milestone achieved in September 2021, NASA and the United States Space Force (USSF) are now actively collaborating to determine the best path forward to make ES-MCAT data accessible to the SSN to support space situational awareness and provide access to under-sampled, low-inclination orbits and new GEO longitudes. ♦

SpaceX Crew-4 Post-flight Meteoroid and Orbital Debris Inspection

J. HYDE AND E. CHRISTIANSEN

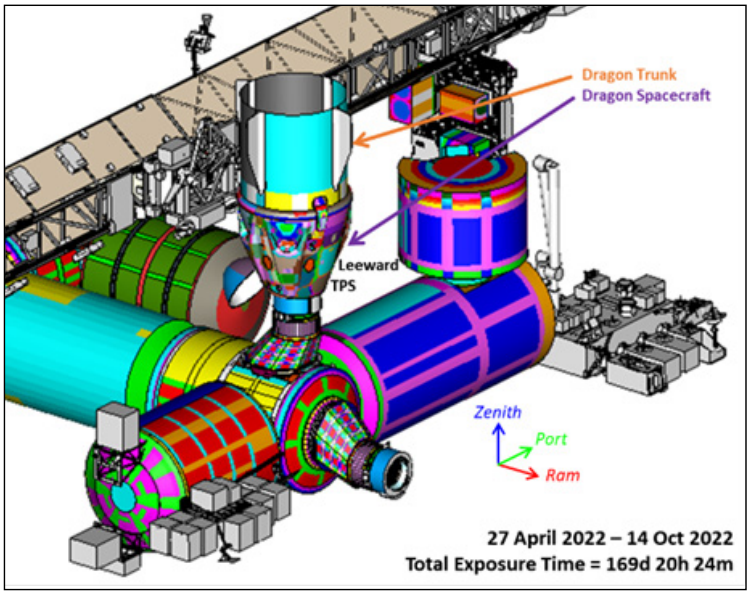

Figure 1. Finite element model of the Crew-4 vehicle on ISS Node 2 zenith docking port.

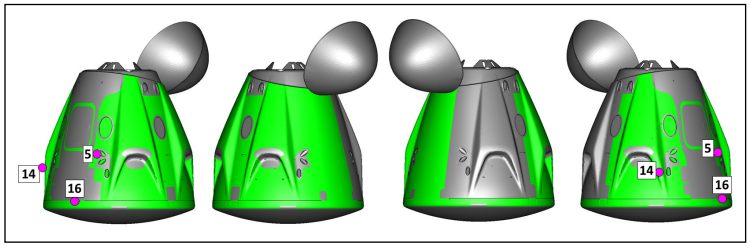

Figure 2. Four side views (90-degree rotations) of the Crew-4 vehicle with inspected regions indicated in green and non-inspected regions shown in gray. Also shown are locations of three impact sites #5, 14 & 16 on the leeward surfaces.

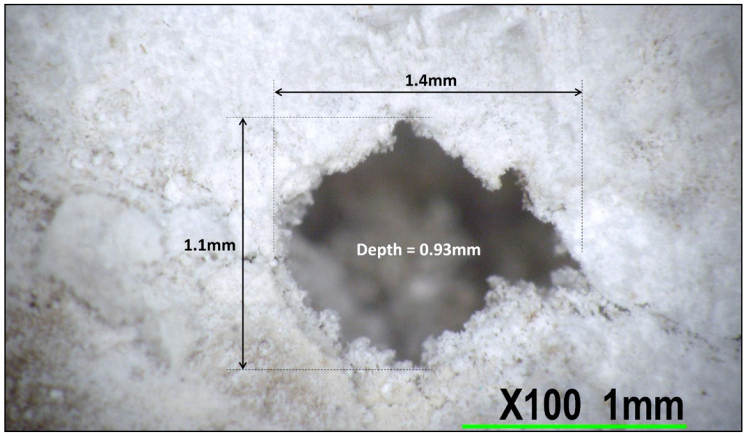

Figure 3. Impact feature #14, observed in the leeward thermal protection system of the Crew-4 vehicle.

A post-flight inspection was performed on the SpaceX Dragon vehicle after the Crew-4 mission for micrometeoroid and orbital debris (MMOD) damage. Fourteen possible MMOD impact damages were identified on the areas of the vehicle inspected. The largest impact damages were extracted for subsequent examination by scanning electron microscopy equipped with x-ray spectrometers to analyze the composition of possible projectile residues and determine if the damage was due to orbital debris or micrometeoroids. The collected data will be used to compare to damage predictions using the Bumper-code and the latest Meteoroid Engineering Model (MEM) 3 and Orbital Debris Engineering Model (ORDEM) 3.2. Along with similar data from other missions, the NASA Orbital Debris Program Office uses this information to understand how well MMOD damage compares to predictions and in building and validating future updates to the environment model provided the latest, available data. The data can also be used by the spacecraft team to evaluate how well the thermal protection system (TPS) performs against the MMOD environment. In the case of Crew-4, all impact damages were well within damage tolerance limits of the TPS, and no issues were encountered from MMOD impact.

The SpaceX Crew-4 mission spent nearly 170 days on the Node 2 zenith docking port of the International Space Station (ISS). Figure 1 illustrates the orientation of the Dragon spacecraft during the Crew-4 mission. This was the initial flight of the Dragon Freedom vehicle (C212), taking place between 27 April and 14 October 2022. After recovery, portions of the spacecraft were inspected for MMOD damage at the SpaceX processing facility at Cape Canaveral Space Force Station in Florida. The initial inspection identified 20 MMOD regions of interest, but after further comparison with preflight imagery and an internal review of the data, the final number of MMOD indications was reduced to 14.

Figure 2 illustrates the capsule regions that were included in the Crew-4 post flight inspection. The green colored areas (with an approximate area of 18.6 m^2) were screened for MMOD damage, while the areas in grey (with an area of 30.0 m^2) were not inspected. The uninspected regions were omitted due to reentry heating effects, nominal vehicle processing, and parachute extraction. The Dragon spacecraft post-flight inspection focused on the back shell TPS. Of the 14 total features recorded, 9 occurred in the TPS, 3 were detected on reaction control system engine nozzles, and 2 were seen on the shoulder region of the base heat shield. The 9 suspected MMOD features in the TPS had an average entry hole size of 1.2 mm × 1.1 mm with an average depth of 0.76 mm. The engine nozzle damage instances had an average coating spall size of 2.3 mm × 2.2 mm each exhibiting a smaller central pit with an average depth of 0.47 mm. The two craters in the base heat shield shoulder averaged 2.3 mm × 2.1 mm in diameter with an average depth of 0.98 mm.

Out of the 14 impact features, 10 impact sites were observed on the TPS-leeward portion of the Dragon spacecraft,

continued on page 7

Crew-4 Inspection

continued from page 6

which was oriented in the ram, or forward-facing, direction of the ISS when docked at Node 2 zenith. Of the four remaining impacts, one occurred on the starboard-facing side, two on the port-facing side, and one on the wake side of the Dragon spacecraft on Node 2 zenith, relative to the ISS velocity direction.

A typical MMOD observation in the Dragon spacecraft TPS is shown in Figure 3. Impact #14 exhibits a frequently seen damage morphology in this type of material: a jagged, irregular entry hole accompanied by a crater volume that expands laterally beyond the original extent of the initial damage feature. As shown in Figure 3, the lateral dimensions of this damage site were 1.4 mm × 1.1 mm from a 100× microscope image. Three depth measurements were recorded using a digital optical micrometer and averaged to give a nominal crater depth of 0.93 mm. Intact extraction sampling of this area was not requested, so information on the source of this impact will not be available.

During the routine on-orbit inspection prior to the return of the Crew-4 vehicle, an area of interest was noted on a thruster nozzle. Figure 4 provides a magnified view of this damage during the post-flight inspection. The damage site is a typical hypervelocity impact into a coated thin metallic wall – a relatively large area of coating spall around a smooth-bottomed hemispherical crater with raised lips. Measurements of the area indicate a coating spall diameter of 3.5 mm with a central pit diameter of 0.814 mm. Two depth measurements of 0.87 mm and 0.77 mm were taken at the central pit giving an average of 0.82 mm. This was the largest damage site observed on the Crew-4 vehicle inspection.

Impact #16 also occurred on the portion of the spacecraft that was facing in the ISS ram direction while docked to Node 2 zenith. This feature was observed on the shoulder region of the base heat shield near the parachute door. A 50× magnification image of the site is provided in Figure 5. Entry hole dimensions of 2.4 mm × 2.2 mm were estimated by scaling from the known dimension watermarked on the image. Three depth measurements were obtained with a digital optical micrometer and averaged to 1.29 mm. Intact extraction sampling of this area was not requested, so information on the source of this impact will not be available.

A comparison between predicted and observed damage is given in Figure 6. The predictions are based on engineering models of the naturally occurring meteoroid environment (MEM 3), the human-made orbital debris environment (ORDEM 3.2), and assumed particle diameters that produced the 14 observed impact features. The red predicted impacts curve was generated from results of the Bumper 3 risk assessment code using a detailed finite element model (FEM) of the Dragon spacecraft. The FEM has been discretized to match areas that may or may not be inspected so that an accurate area is used in the calculation. Mission duration and exposure year are also considered in the predictions. In general, this mission saw somewhat more impact damage than predicted above 0.3 mm diameter particle diameter, but all observed impact damage was well below critical damage thresholds. ♦

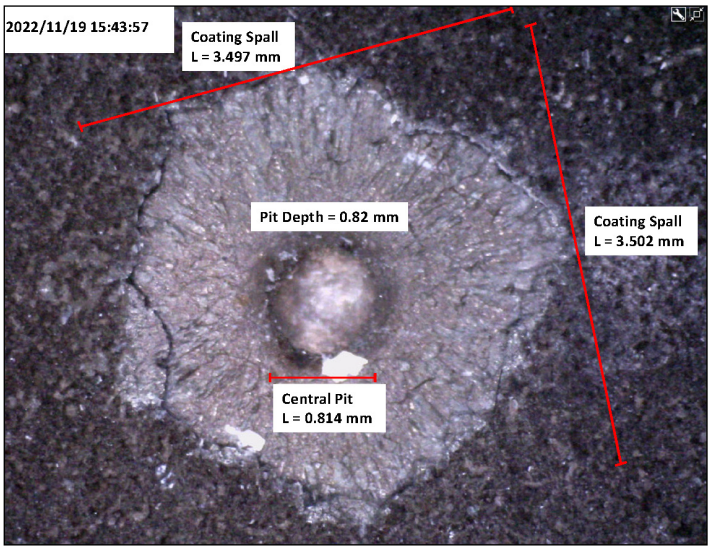

Figure 4. Impact feature #5, observed on reaction control system engine nozzle of the Crew-4 vehicle. The unit magnification is 59.3×.

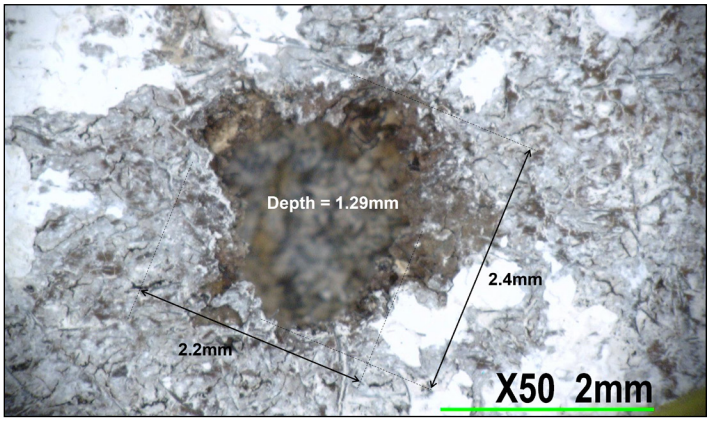

Figure 5. Impact feature #16, observed in leeward heat shield shoulder of the Crew-4 vehicle.

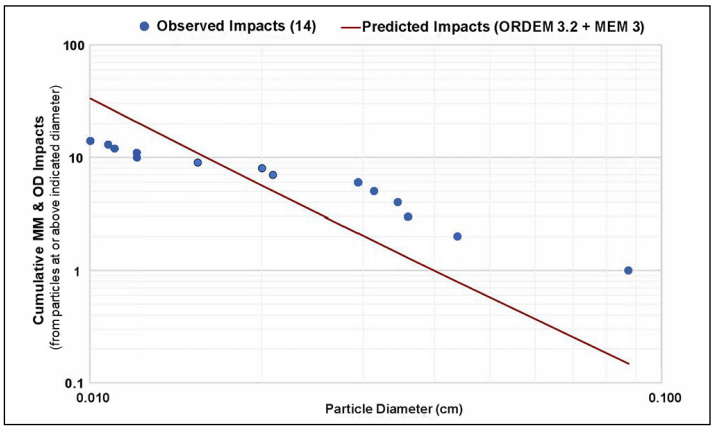

Figure 6. As-flown comparison of observed impacts and model predictions using the Bumper 3 code with ORDEM 3.2 and MEM 3 environments.

Goldstone Orbital Debris Radar Measurements of the Orbital Debris Environment: 2020 to 2021

J. MURRAY, M. MATNEY, AND A. MANIS

For nearly 30 years, the NASA Orbital Debris Program Office (ODPO) has used the Goldstone Orbital Debris Radar (Goldstone) to characterize the orbital debris (OD) in low Earth orbit (LEO) too small to be tracked by the U.S. Space Surveillance Network. Goldstone is operated by NASA's Jet Propulsion Laboratory and can detect OD as small as 3 mm for altitudes up to 1000 km. It is the most sensitive radar used for these types of measurements and provides the ODPO with unique and important insights on small OD in LEO.

The data collected by Goldstone is used for the development and validation of debris populations for the NASA Orbital Debris Engineering Model (ORDEM). Due to the dynamic nature of the OD environment, measurements are performed on an ongoing basis to update ORDEM as the environment evolves. This review describes a new pointing plan developed for Goldstone and an overview of radar data collected in calendar year (CY) 2020 to 2021. A detailed report on the most recent Goldstone observations from CY 2020-2021 will be published soon [1].

Goldstone is a bistatic radar and performs measurements in a beampark mode in which the transmitter is pointed at a fixed azimuth and elevation, the receiver is pointed to intersect the transmitter beam at a target slant range, and objects are detected as they pass through the common volume of the transmitter and receiver beams. For 25 years, orbital debris operations utilized Goldstone's Deep Space Station (DSS) sensors, specifically DSS-14 as a transmitter and DSS-15 as a receiver, to provide a short baseline for beam overlap for all of LEO with a single pointing geometry. In early 2018, DSS-15 was decommissioned and replaced with DSS-25 (and occasionally DSS-26) of the Deep Space Network Apollo Cluster. This increased the bistatic baseline from approximately 500 m to approximately 10 km. The instantaneous bistatic beam overlap was significantly reduced, requiring altitudes of interest to be targeted. Observations in CY2018 focused on an approximately 100 km wide altitude window centered at 800 km slant range from DSS-14, as this is approximately the region of highest small-OD flux (ODQN, vol. 23, issue 1 & 2, pp. 8, 2019) [2]. In 2019, DSS-14 was offline for maintenance, and the ODPO designed an annual survey observation plan to sample altitudes from 700 km to 1000 km efficiently, since many NASA satellites populate this range. It was determined that four overlapping pointings could be used to optimize coverage over the altitude regime of interest without significant sensitivity loss relative to the legacy system at any given pointing. This new observation plan was implemented for measurements beginning in CY2020.

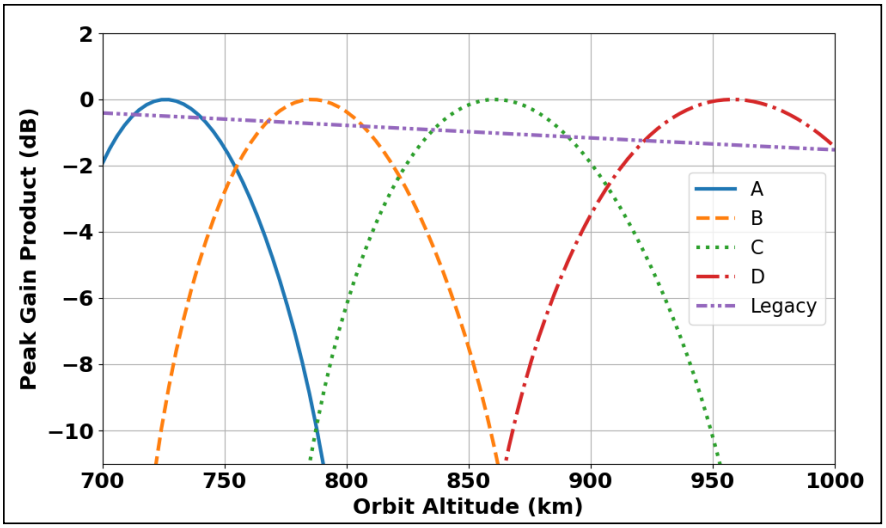

Figure 1. Peak gain product versus orbit altitude of the A, B, C, D, and Legacy pointings showing the extent of their bistatic beam overlaps.

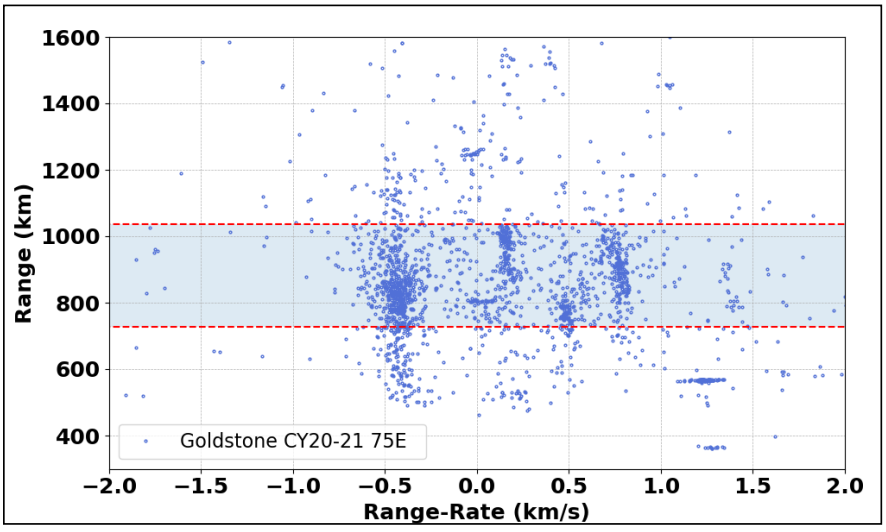

Figure 2. Range versus range-rate observations, measured by Goldstone in CY2020 to 2021. The horizontal dashed lines and shaded region represent the 700 km to 1000 km altitude window of interest, which corresponds to 728 km to 1037 km in range.

Figure 1 shows the peak gain product of the bistatic beam overlap as a function of orbit altitude for each of the four pointings, named A, B, C, and D, in the observation plan. The pointings were chosen to be no more than 1.5 dB less sensitive than the legacy system at any given altitude. In fact, the new pointings are more sensitive near the targeted altitudes than the legacy system due

continued on page 9

Goldstone Measurements

continued from page 8

to the nature of the bistatic overlap. In all the pointings, A, B, C, and D, the transmitter is pointed at 75° due East, or 75E. The fundamental measurements made by the radar are range, range-rate, and received power from which radar cross-section (RCS) can be calculated. Figure 2 shows a plot of the range and range-rates measured for all detections at all pointings in CY2020 to 2021 as well as horizontal lines that indicate the altitude extent of interest. Many detections exist beyond this altitude window, corresponding to objects large enough to pass through the sidelobes of the radar beams and still be detected.

Assuming a circular orbit, the inclinations of objects traveling through the beam can be estimated using the measured range and range-rate, or Doppler velocity. This allows the transformation of the data from range and range-rate to orbit altitude and Doppler inclination, as shown in Figure 3. Several debris families can be identified in Figure 3, the largest being the sun-synchronous family of orbits clustered around the dashed black line indicating the sun-synchronous inclinations for circular orbits. Several notable on-orbit fragmentation events are also noted with black circles, the centers of which correspond to the altitude and inclination of the parent body at the time of the event. A black ellipse encircles detections associated with the Starlink satellite constellation at approximately 53° inclination, all of which are outside the 700 km to 1000 km target altitudes indicated by the horizontal dashed lines and shaded region.

The RCS of an object is calculated from the power of the reflected signal and the range of the object. The size of a debris object can be estimated from the measured RCS using the NASA Size Estimation Model (SEM) [3]. Figure 4 shows a plot of altitude versus the SEM-estimated size for Goldstone detections in CY2020 to 2021. A dashed black curve is also included, indicating the altitude dependent size to which the data is estimated to be 99% complete; 99% of objects of that size and larger passing through the beam are detected. The dotted black curve shows the equivalent completeness curve for data taken by Goldstone in CY2016 using the legacy configuration. The horizontal dashed lines and shaded region again represent the 700 km to 1000 km target altitudes. The data at small sizes follows the completeness curve in this region, with detection efficiency falling off rapidly outside the main beam overlaps.

The newly developed observation plan has yielded some of the most sensitive measurements of OD in LEO made with terrestrial radar to date. With this new plan, the minimum completeness size is now approximately 2.2 mm at 1000 km altitude. Continued radar measurements with Goldstone will provide valuable information on OD in the few-millimeter size regime from 700 km to 1000 km in altitude.

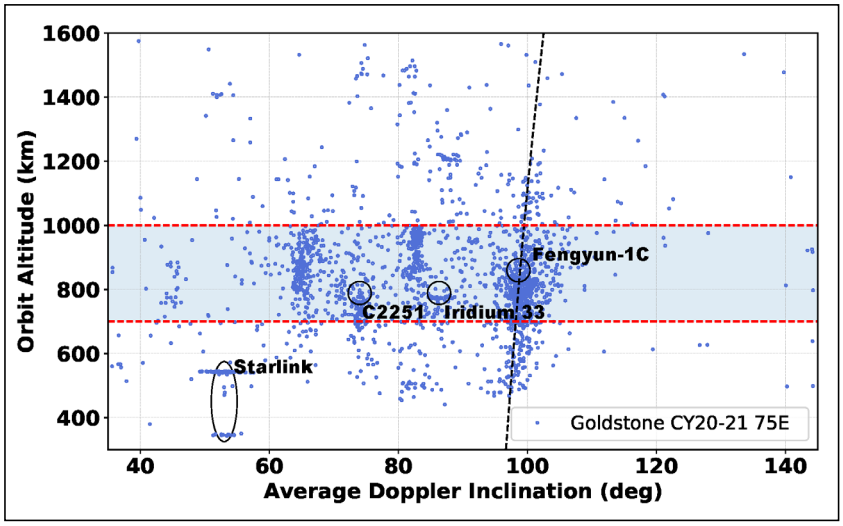

Figure 3. Conversion of Goldstone CY2020 to 2021 range and range-rate measurements into orbit altitude and Doppler-derived inclination. The sun-synchronous condition, assuming a circular orbit, is shown by the dashed black curve.

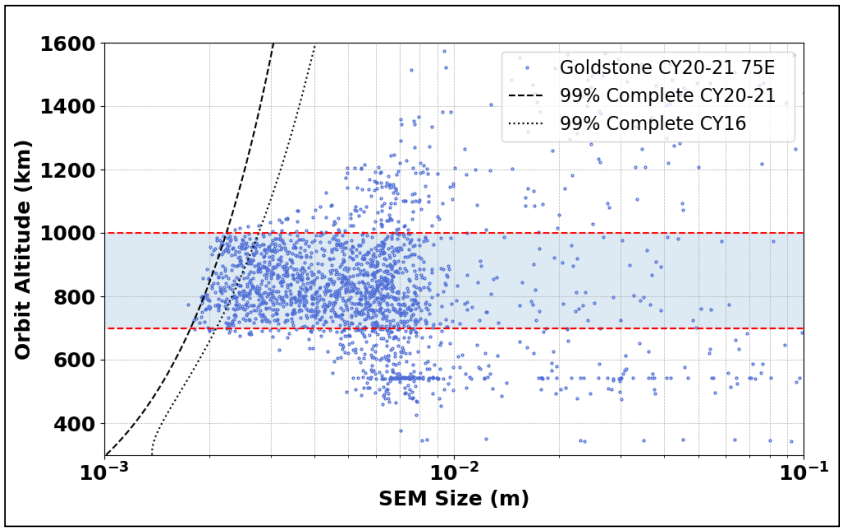

Figure 4. Orbit altitude versus SEM-size, measured by Goldstone in CY2020 to 2021. The dashed and dotted black curves represent the altitude dependent size to which the CY2020 to 2021 and CY2016 data, respectively, are estimated to be 99% complete.

References

1. Murray, J. and Matney, M. "Goldstone Radar Measurements of the Orbital Debris Environment: 2020-2021," NASA Technical Publication, In-work.
2. Miller, R. *et al*. "Goldstone Radar Measurements of the Orbital Debris Environment: 2018," NASA/TP-20210015780, April 2021.
3. Xu, Y.-L. and Stokely, C. "A Statistical Size Estimation Model for Haystack and HAX Radar Detections," *56th International Astronautical Congress*, Fukuoka, Japan, (2005). ♦

MEETING REPORTS

The NASA-DOD Orbital Debris Working Group Meeting, 16 November 2022, Virtual

The 25th annual NASA-DOD Orbital Debris Working Group (ODWG) was held virtually on 16 November 2022. This annual one-day meeting provides the framework for cooperation and collaboration between NASA and the DOD on orbital debris-related activities, such as measurements, modeling, mitigation, and policy development. NASA and the DOD have benefited significantly from this group, and many collaborations directly result from it. The meeting was co-chaired by the NASA Orbital Debris Program Office (ODPO) and by the Operational Assessments Division, HQ Space Operations Command, United States Space Force (USSF).

The USSF and the NASA ODPO provided opening remarks, followed by a series of presentations by members representing NASA and DOD. The NASA ODPO provided an update on the development and future enhancements being integrated into the next-generation Orbital Debris Engineering Model, ORDEM 4.0. This presentation was followed by an update on the DebriSat project and the fusion of measurements and analysis from the project into the next generation ORDEM 4.0 and NASA Standard Satellite Breakup Model.

Two ODPO presentations on radar and optical measurement activities were presented. The initial presentation discussed the low Earth orbit debris environment as revealed by recent measurements from the Haystack Ultra-Wideband Satellite Imaging Radar (HUSIR) and the Goldstone Orbital Debris Radar, including the special measurement campaign following the intentional destruction of the Cosmos 1408 spacecraft in November 2021. The NASA ODPO then offered an update on the Eugene Stansbery Meter-Class Autonomous Telescope (ES-MCAT). The ES-MCAT concluded its first complete survey of the geosynchronous region in February 2022. The final ODPO presentation outlined details of the Object Reentry Survival Analysis Tool (ORSAT) 7.0, released in October 2022, including the newly implemented charring ablation model for fiber-reinforced plastic materials and drag and heating models for hollow objects. Closing the formal NASA presentations, an overview of the meteoroid environment, which dominates the risk for the increasing number of missions proposed and operated in cislunar and lunar space, was given by the NASA Meteoroid Environment Office.

DOD personnel presented an overview of the reentry prediction process followed by the 18th Space Defense Squadron (18SDS, formerly 18th Space Control Squadron) at Vandenberg Space Force Base. Following this presentation, the USSF reviewed the confirmed breakups since October 2021, including the anti-satellite test conducted against Cosmos 1408 (International Designator 1982-092A, Catalog number 13552), a Minotaur IV rocket body (International Designator 2020-046E, Catalog number 45877), another piece of H-IIA mission related debris (2018-084D, 46374), Orbcomm FM 5 (1997-084F, 25117), an SL-4 rocket body (2006-061B, 29669), the 53rd breakup of a SOZ rocket (2007-065F, 32398), and the very recent breakup of a Long March 6A (CZ-6A) rocket body (2022-151B, 54236). These breakups were previously reported in ODQN vol. 26, issue 1, 2, and 4, March/July/December 2022, pp. 1-5, 2-5, and 1-2, respectively.

Following the overview of recent breakups, the DOD presented details on the response of the 18SDS to the breakup of Cosmos 1408, including the rapid cataloging of fragments in the debris cloud and their incorporation into conjunction assessments. DOD personnel presented a Space Surveillance Telescope update as it proceeded through initial operating capability to operational acceptance into the Space Surveillance Network in September 2022. The final DOD presentation, from the Air Force Research Laboratory, discussed research and operational updates in their efforts to improve tracking and debris mitigation in cislunar space. ♦

The 12th Ablation Workshop, 09-10 November 2022, Lexington, Kentucky

The annual Ablation Workshop was hosted by the University of Kentucky, Lexington, after a three-year hiatus, on 09-10 November 2022. This event was sponsored by Analytical Mechanics Associates, Sandia National Laboratories, University of Kentucky, and the NASA Kentucky Space Grant Consortium and Established Program to Stimulate Competitive Research programs. The workshop is a forum for researchers to share recent advances in modeling and experimental results relating to pyrolysis and ablation of materials in high-enthalpy flows.

The workshop consisted of a single track with technical sessions covering material response modeling at multiple length scales, flight experiments, plasma wind tunnel experiments, and model validation. Highlighted topics included modeling pyrolysis and material response of woven carbon-fiber thermal protection systems (TPS), a relatively untested technology in the atmospheric entry systems field. This topic pertains to the demisability of carbon fiber composite structures on many modern spacecraft, making it of particular interest to the ODPO.

In addition to the presentations, the workshop hosted a poster session on topics ranging from the design of a laser-driven tabletop shock tunnel to using x-ray micro-computed tomography scans to characterize the thermal properties of TPS materials. A subset of presentations can be accessed at https://ablation.engr.uky.edu/presentations. ♦

SUBSCRIBE to the ODQN or UPDATE YOUR SUBSCRIPTION ADDRESS

To be notified when a new issue of the ODQN is published or to update your email address, subscribe on the NASA Orbital Debris Program Office (ODPO) website at: https://orbitaldebris.jsc.nasa.gov/quarterly-news/

UPCOMING MEETINGS

24-27 April 2023: 2023 CubeSat Developers Workshop, San Luis Obispo, California, USA

The CubeSat Developers Workshop is an annual three-day meeting hosted by Cal Poly CubeSat Laboratory focused on small satellite development. The workshop provides a forum for industry professionals, small satellite developers, and students to engage with various aspects of CubeSat design, development, and operations. The abstract submission closed on 01 February 2023. Additional details on the workshop can be found at https://www.cubesatdw.org/.

05-10 August 2023: 37th Small Satellite Conference, Logan, Utah, USA

Utah State University (USU) and the American Institute of Aeronautics and Astronautics (AIAA) will sponsor the 37th Annual USU/AIAA Conference on Small Satellites under the theme "Missions Small at Satellite Scale." This conference will explore future missions and delve into key technology drivers, operational constructs, and activities that inform and secure success of small satellite missions at scale. The call for papers ended on 02 February 2023. Conference information is available at https://smallsat.org/.

19-22 September 2023: 24th Advanced Maui Optical and Space Surveillance Technologies Conference (AMOS), Maui, Hawaii, USA

The technical program of the 24th Advanced Maui Optical and Space Surveillance Technologies Conference (AMOS) will focus on subjects that are mission critical to space situational awareness. The technical sessions include papers and posters on orbital debris, space situational/space domain awareness, adaptive optics and imaging, astrodynamics, non-resolved object characterization, and related topics. The abstract submission deadline was 01 March 2023. Additional information about the conference is available at https://amostech.com.

02-06 October 2023: 74th International Astronautical Congress (IAC), Baku, Azerbaijan

The IAC will convene in 2023 with a theme of "Global Challenges and Opportunities: Give Space a Chance." Of note, the 24th IAC was last held in Baku almost 50 years ago in 1973. The IAC's 21st International Academy of Astronautics Symposium on Space Debris will cover debris measurements and characterization; modeling; risk analysis; hypervelocity impact and protection; mitigation; post-mission disposal; space debris mitigation and removal; operations in the space debris environment; political and legal aspects of mitigation and removal; orbit determination and propagation; and financial gains with space debris. This year, the IAC will offer a venue for interactive presentations on space debris topics to allow more digital display capabilities for attendees. The abstract submission deadline passed on 28 February 2023. Additional information for the 2023 IAC is available at https://www.iafastro.org/events/iac/iac-2023/ and http://iac2023.org/. ♦

The 2nd International Orbital Debris Conference (IOC) is scheduled for December 4–7, 2023. The conference goal is to highlight orbital debris research activities in the United States and to foster collaborations with the international community. The four-day conference will cover all aspects of micrometeoroid and orbital debris research, mission support, and other activities.

The deadline for the submission of abstracts is **March 30, 2023.**

https://www.hou.usra.edu/meetings/orbitaldebris2023/

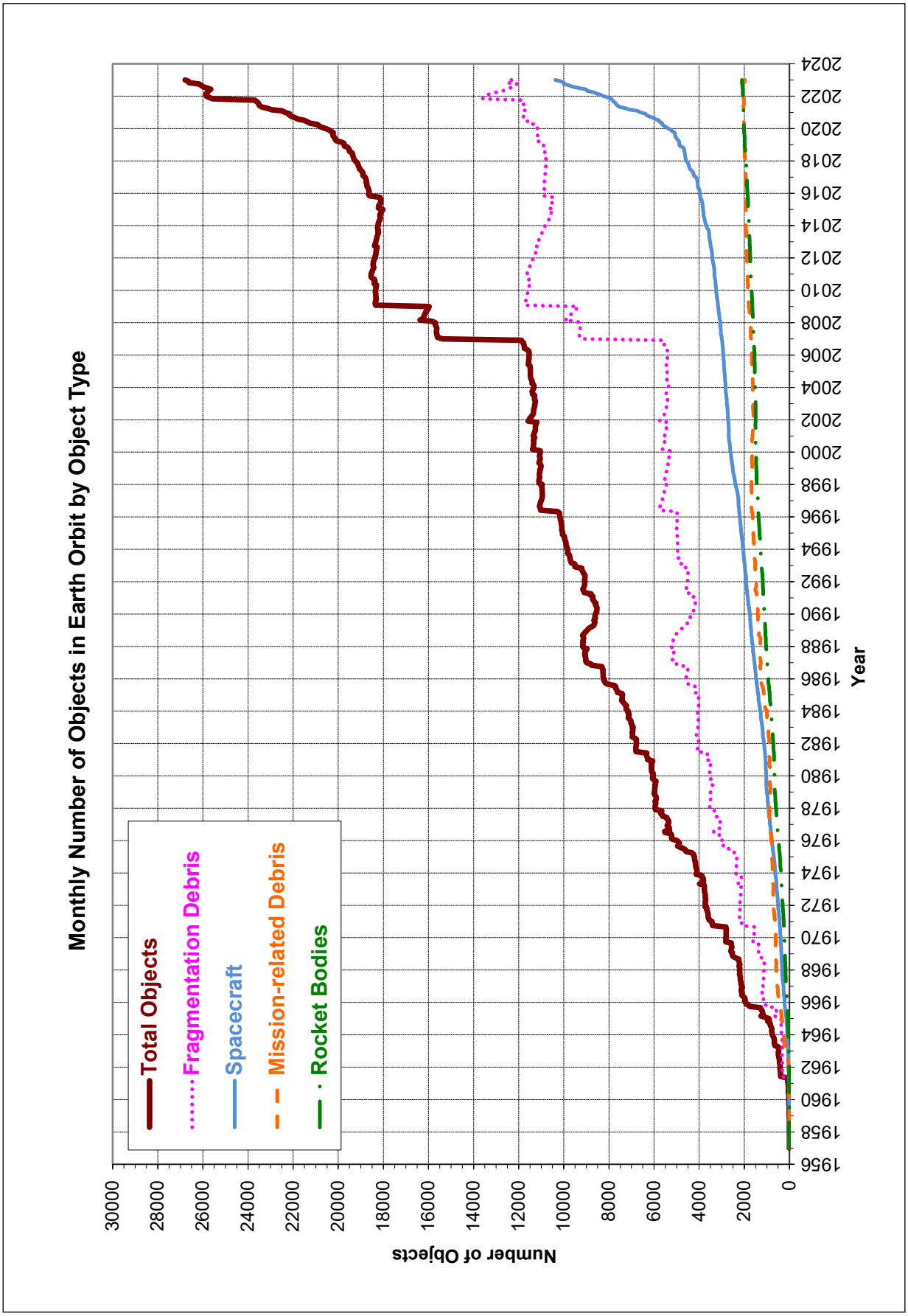

Monthly Number of Cataloged Objects in Earth Orbit by Object Type as of 03 February 2023. This chart displays a summary of all objects in Earth orbit officially cataloged by the U.S. Space Surveillance Network. "Fragmentation debris" includes satellite breakup debris and anomalous event debris, while "mission-related debris" includes all objects dispensed, separated, or released as part of the planned mission

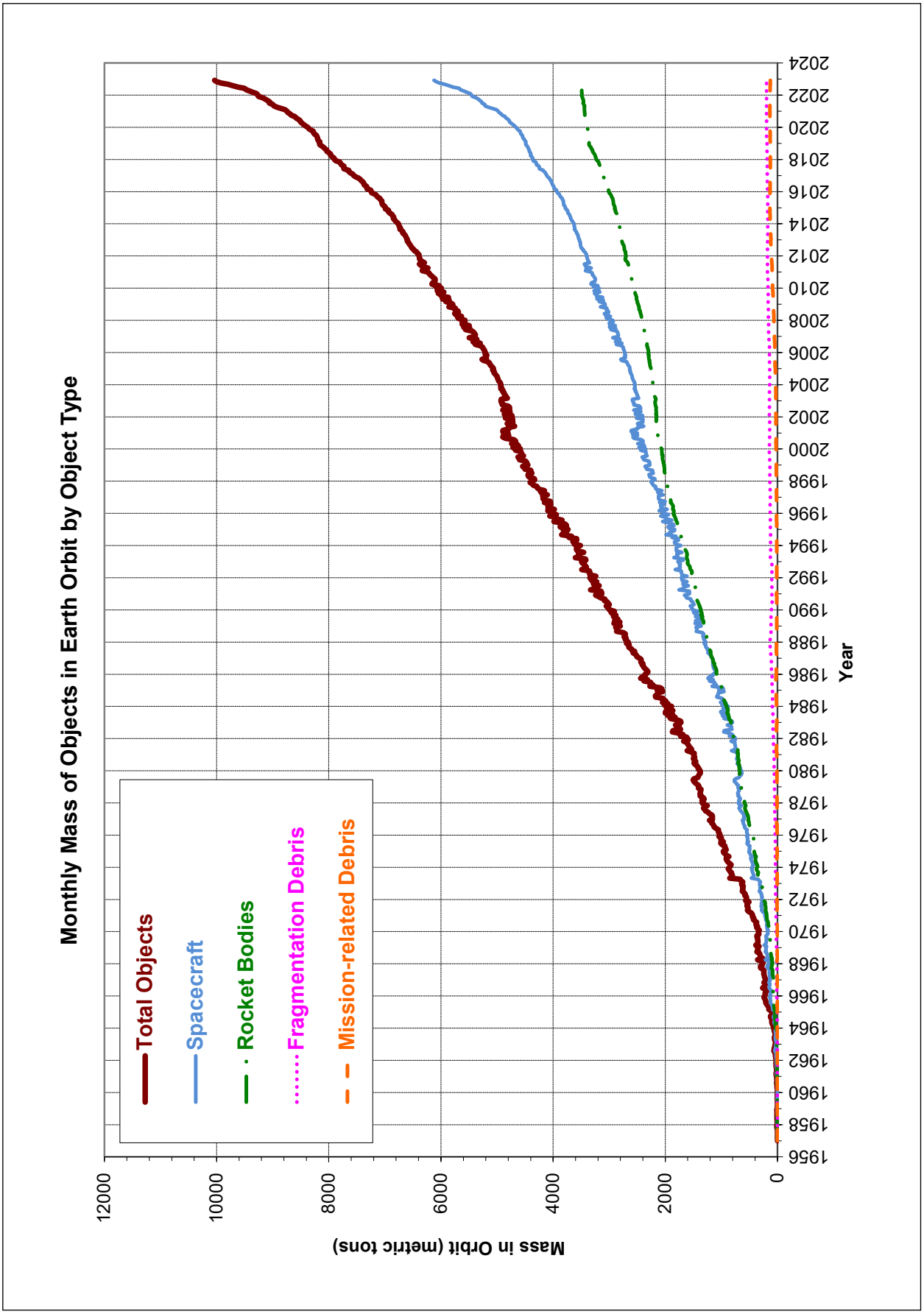

Monthly Mass of Objects in Earth Orbit by Object Type as of 03 February 2023. This chart displays the mass of all objects in Earth orbit officially cataloged by the U.S. Space Surveillance Network.

SATELLITE BOX SCORE

(as of 04 February 2023, cataloged by the U.S. SPACE SURVEILLANCE NETWORK)

Country/ Organization	Spacecraft*	Spent Rocket Bodies & Other Cataloged Debris	Total
CHINA	604	4299	4903
CIS	1564	5970	7534
ESA	96	57	153
FRANCE	84	516	600
INDIA	111	105	216
JAPAN	209	112	321
UK	595	1	596
USA	5718	5172	10890
OTHER	1152	92	1244
Total	10133	16324	26457

* active and defunct

Visit the NASA
Orbital Debris Program Office Website
www.orbitaldebris.jsc.nasa.gov

Technical Editor
Heather Cowardin, Ph.D.

Managing Editor
Ashley Johnson

Correspondence can be sent to:

Robert Margetta
robert.j.margetta@nasa.gov

or to:

Nilufar Ramji
nilufar.ramji@nasa.gov

National Aeronautics and Space Administration
Lyndon B. Johnson Space Center
2101 NASA Parkway
Houston, TX 77058

www.nasa.gov
https://orbitaldebris.jsc.nasa.gov/

Intl. = International; SC = Spacecraft; Alt. = Altitude; Incli. = Inclination; Addnl. = Additional; R/B = Rocket Bodies; Cat. = Cataloged
Notes: 1. Orbital elements are as of data cut-off date 31 December. 2. Additional spacecraft on a single launch may have different orbital elements. 3. Additional uncatalogued objects may be associated with a single launch.

INTERNATIONAL SPACE MISSIONS

01 October 2022 – 31 December 2022

Intl.* Designator	Spacecraft	Country/ Organization	Perigee Alt. (KM)	Apogee Alt.(KM)	Incli. (DEG)	Addnl. SC	Earth Orbital R/B	Other Cat. Debris
1998-067	ISS dispensed objects	Various	412	423	51.6	12	0	0
2022-122A	OBJECT A	TBD	160	175	136.9	3	1	0
2022-123A	SES 20	SES	35779	35792	0.1	0	1	0
2022-123B	SES 21	SES	35782	35791	0.0			
2022-124A	DRAGON ENDURANCE 2	US	412	423	51.6	0	0	0
2022-125A	STARLINK-4633	US	539	541	53.2	51	0	4
2022-126A	CENTISPACE-1 S5	PRC	687	708	55.0	0	1	0
2022-126B	CENTISPACE-1 S6	PRC	686	710	55.0			
2022-127A	OTB-3-GAZELLE	US	744	762	98.3	0	2	0
2022-128A	GALAXY 33	US	35778	35795	0.0	0	1	0
2022-128B	GALAXY 34	US	35777	35796	0.0			
2022-129A	ASO-S	PRC	713	732	98.3	0	1	0
2022-130A	COSMOS 2559 (GLONASS)	CIS	19113	19147	64.8	0	1	0
2022-131A	ANGOSAT 2	AGO	35787	35787	0.0	0	1	0
2022-132A	HJ-2E	PRC	480	496	97.4	0	1	5
2022-133A	YAOGAN-36 02A	PRC	490	500	35.0	0	1	1
2022-133B	YAOGAN-36 02B	PRC	488	502	35.0			
2022-133D	YAOGAN-36 02C	PRC	487	502	35.0			
2022-134A	HOTBIRD 13F	EUTE	EN ROUTE TO GEO			0	1	0
2022-135A	COSMOS 2560	CIS	130	150	96.3	0	0	0
2022-136A	STARLINK-5195	US	539	541	53.2	53	0	4
2022-137A	COSMOS 2561	CIS	398	411	97.1	0	2	0
2022-137B	COSMOS 2562	CIS	376	391	97.2			
2022-138A	ONEWEB-0490	UK	1185	1187	87.9	35	1	0
2022-139A	GONETS-M 23	CIS	1477	1511	82.5	0	1	0
2022-139B	GONETS-M 24	CIS	1481	1508	82.5			
2022-139C	GONETS-M 25	CIS	1478	1511	82.5			
2022-139D	SKIF-D	CIS	8050	8069	90.0			
2022-140A	PROGRESS MS-21	CIS	412	423	51.6	0	1	0
2022-141A	STARLINK-5290	US	539	541	53.2	52	0	4
2022-142A	SHIYAN 20C (SY-20C)	PRC	781	812	60.0	0	1	0
2022-143A	CSS (MENGTIAN)	PRC	383	386	41.5	0	1	0
2022-144A	LDPE-2	US	NO ELEMS AVAILABLE			5	1	1
2022-145A	COSMOS 2563	CIS	1499	38860	63.8	0	1	0
2022-146A	HOTBIRD 13G	EUTE	EN ROUTE TO GEO			0	1	0
2022-147A	MATS	SWED	579	598	97.7	0	2	0
2022-148A	CHINASAT 19	PRC	35757	35817	0.0	0	1	0
2022-149A	CYGNUS NG-18	US	412	423	51.6	0	1	0
2022-150A	NOAA 21	US	826	828	98.7	0	0	0
2022-151A	YUNHAI 3	PRC	847	849	98.8	0	1	0
2022-152A	TIANZHOU 5	PRC	383	386	41.5	0	1	4
2022-152D	CZ-7 R/B	PRC	143	152	41.5			
2022-153A	GALAXY 31	US	35772	35800	0.1	0	1	0
2022-153B	GALAXY 32	US	35655	35681	0.0			
2022-154A	YAOGAN-34 03	PRC	1082	1097	63.4	0	0	0
2022-155A	OBJECT A	PRC	525	545	97.5	0	0	0
2022-155B	OBJECT B	PRC	525	545	97.5			
2022-155C	OBJECT C	PRC	526	546	97.5			
2022-155D	OBJECT D	PRC	525	545	97.5			
2022-155E	OBJECT E	PRC	525	544	97.5			
2022-156A	ORION	US	LUNAR & RETURN ORBIT					
2022-157A	EUTELSAT 10B	EUTE	EN ROUTE TO GEO			0	1	0
2022-158A	EOS-6	IND	734	737	98.4	8	0	0
2022-158B	OBJECT B	TBD	497	530	97.5			
2022-159A	DRAGON CRS-26	US	213	370	51.7	0	0	1
2022-160A	OBJECT A	PRC	492	499	35.0	0	0	0
2022-160B	OBJECT B	PRC	480	489	35.0			
2022-160C	OBJECT C	PRC	492	500	35.0			
2022-160D	OBJECT D	PRC	477	487	35.0			
2022-160E	OBJECT E	PRC	491	500	35.0			
2022-161A	COSMOS 2564 (GLONASS)	CIS	19113	19147	64.8	0	1	0
2022-162A	SZ-15	PRC	383	386	41.5	0	1	0
2022-163A	COSMOS 2565	CIS	900	910	67.2	0	1	0
2022-163C	OBJECT C	CIS	893	913	67.1			
2022-163D	OBJECT D	CIS	894	915	67.1			
2022-164A	OBJECT A	PRC	736	751	98.4	0	1	0
2022-165A	GAOFEN 5 01A	PRC	699	701	98.1	0	1	0
2022-166A	ONEWEB-0527	UK	735	749	86.8	39	0	0
2022-167A	OBJECT A	PRC	526	545	97.5	13	0	0
2022-167B	OBJECT B	PRC	298	553	97.6			
2022-168A	HAKUTO-R M1	JPN	EN ROUTE TO MOON			0	0	0
2022-168B	LUNAR FLASHLIGHT	US	EN ROUTE TO 12 HOUR MEO					
2022-169A	OBJECT A	PRC	791	801	60.0	0	0	0
2022-169B	OBJECT B	PRC	787	805	60.0			
2022-169C	OBJECT C	PRC	658	796	60.0			
2022-169D	OBJECT D	PRC	788	801	60.0			
2022-170A	GALAXY 35	US	35776	35797	0.1	0	1	1
2022-170B	GALAXY 36	US	35590	35609	0.0			
2022-170C	METEOSAT 12 (MTG I1)	EUME	35779	35798	0.9			
2022-171A	OBJECT A	PRC	493	499	35.0	0	0	0
2022-171B	OBJECT B	PRC	483	489	35.0			
2022-171C	OBJECT C	PRC	493	500	35.0			
2022-171D	OBJECT D	PRC	481	487	35.0			
2022-171E	OBJECT E	PRC	488	504	35.0			
2022-172A	SHIYAN 21 (SY-21)	PRC	464	502	36.0	0	0	0
2022-173A	SWOT	US	859	860	77.6	0	0	0
2022-174A	SES MPOWER-A F1	SES	EN ROUTE TO 4.7 HOUR MEO			0	1	0
2022-174B	SES MPOWER-A F2	SES	EN ROUTE TO 4.7 HOUR MEO					
2022-175A	STARLINK-5464	US	490	492	53.2	53	0	4
2022-176A	GAOFEN 11 04	PRC	239	610	97.3	0	1	0
2022-177A	STARLINK-5382	US	524	526	43.0	53	0	4
2022-178A	SHIYAN 10 02 (SY-10 02)	PRC	1781	38574	63.3	0	1	0
2022-179A	EROS C3	ISRA	482	497	139.4	0	1	0